Polarization-Dependent Sum-Frequency Generation Spectroscopy for Ångstrom-Scale Depth Profiling of Molecules at Interfaces

Chun-Chieh Yu,* Takakazu Seki,* Yongkang Wang, Mischa Bonn,† and Yuki Nagata‡
Molecular Spectroscopy Department, Max Planck Institute for Polymer Research, Ackermannweg 10, Mainz 55128, Germany

(Received 20 December 2021; revised 28 February 2022; accepted 8 April 2022; published 1 June 2022)

The three-dimensional spatial distribution of molecules at soft matter interfaces is crucial for processes ranging from membrane biophysics to atmospheric chemistry. While several techniques can access surface composition, obtaining information on the depth distribution is challenging. We develop a noninvasive, polarization-resolved, surface-specific sum-frequency generation spectroscopy providing quantitative depth information. We demonstrate the technique on formic acid molecules at the air-water interface. With increasing molar fraction from 2.5% to 10%, the formic acid molecules shift, on average, ∼0.9 Å into the bulk. The consistency with the simulation data manifests that the technique allows for probing the Ångstrom-scale depth profile.

DOI: 10.1103/PhysRevLett.128.226001

Depth information of molecules at interfaces is essential for unveiling many physical, chemical, and biological phenomena, such as the premelting layers of ice surface [1–3] and the propensity of proteins at membrane interfaces [4–6]. Several experimental techniques, including atomic force microscope (AFM) [7], secondary ion mass spectrometry (SIMS) [8], and x-ray photo-electron spectroscopy [9], have been used for capturing the depth profile of molecules at interfaces. Notwithstanding the success of these methodologies, they do typically impose constraints on the studied interfaces and/or can be somewhat invasive. The AFM tip and ions used in SIMS can perturb the surface; optical techniques such as ellipsometry are noninvasive, whereas its probe resolution is usually >5 nm [10]. An all-optical technique to noninvasively obtain molecular-scale interfacial depth information is highly desirable to unveil the molecular structure at surfaces and (buried) interfaces.

Sum-frequency generation (SFG) spectroscopy is a noninvasive, interface-specific, and molecular-specific technique. SFG uses infrared (IR) and visible light to drive a second-order optical process, typically occurring only at interfaces, since second-order processes are prohibited in the bulk of media with centrosymmetry. Thus, SFG spectroscopy possesses interface specificity and is noninvasive. An SFG signal is enhanced when the IR frequency is resonant with a vibrational mode, providing molecular specificity. Thanks to its unique characteristics, SFG has been used for probing the structure and dynamics of interfacial molecules [11,12] and chemical and biological processes occurring at the interface [13,14]. On the other hand, SFG has been recognized as a tool that cannot access quantitative depth information, although some attempts to qualitatively access to the depth information via SFG have been made [15–17]. SFG would be much more powerful if it could be endowed with depth resolution, in addition to its interface and molecule specificity.

Here, we present a technique for obtaining depth information on vibrational chromophores at an Ångstrom-scale by analyzing SFG spectra recorded at different polarization combinations. Extending this polarization-dependent (PD) technique to the heterodyne-detected SFG (HD-SFG) spectroscopy, we demonstrate that SFG signals can report on depth information of the interfacial molecules. This approach reveals the depth distribution of formic acid molecules at the interface of an aqueous formic acid solution with air. Our analysis shows that the C─H groups of formic acid molecules reposition from the subsurface toward the bulk, with increasing molar fraction (x_{FA}). We discuss the possible mechanism underlying the transposition of the formic acid molecules at the interface.

Measured PD-SFG ($\chi^{(2)}_{\mathrm{eff}}$) spectra at the ssp, sps, and ppp polarization combinations, where abc polarization represents the a-, b-, and c-polarized SFG, visible, and IR beams, respectively, are connected with the second-order nonlinear susceptibility ($\chi^{(2)}$) via

$$\chi^{(2)}_{\mathrm{eff},ssp}(\omega_{\mathrm{IR}};\varepsilon') = L_{yy}(\omega_{\mathrm{SFG}})L_{yy}(\omega_{\mathrm{Vis}})L_{zz}(\omega_{\mathrm{IR}};\varepsilon')\sin\beta_{\mathrm{IR}}\chi^{(2)}_{yyz}(\omega_{\mathrm{IR}}), \quad (1)$$

$$\chi^{(2)}_{\mathrm{eff},sps}(\omega_{\mathrm{IR}};\varepsilon') = L_{yy}(\omega_{\mathrm{SFG}})L_{zz}(\omega_{\mathrm{Vis}};\varepsilon')L_{yy}(\omega_{\mathrm{IR}})\sin\beta_{\mathrm{Vis}}\chi^{(2)}_{yzy}(\omega_{\mathrm{IR}}), \quad (2)$$

$$\chi^{(2)}_{\mathrm{eff},ppp}(\omega_{\mathrm{IR}};\varepsilon') \approx -L_{xx}(\omega_{\mathrm{SFG}})L_{xx}(\omega_{\mathrm{Vis}})L_{zz}(\omega_{\mathrm{IR}};\varepsilon') \times \cos\beta_{\mathrm{SFG}}\cos\beta_{\mathrm{Vis}}\sin\beta_{\mathrm{IR}}\chi^{(2)}_{xxz}(\omega_{\mathrm{IR}}) + L_{zz}(\omega_{\mathrm{SFG}};\varepsilon')L_{zz}(\omega_{\mathrm{Vis}};\varepsilon')L_{zz}(\omega_{\mathrm{IR}};\varepsilon') \times \sin\beta_{\mathrm{SFG}}\sin\beta_{\mathrm{Vis}}\sin\beta_{\mathrm{IR}}\chi^{(2)}_{zzz}(\omega_{\mathrm{IR}}), \quad (3)$$

where β_j is the angle of beam j with the surface normal. $L_{ii}(i = x, y, z)$ is the Fresnel factor [18], and ε' is the interfacial dielectric constant. The xz plane forms the incident plane of the beams, and the z axis is defined as the surface normal. For the functional group with the $C_{\infty v}$ symmetry at an azimuthally isotropic interface, the peak amplitudes in the $\mathrm{Im}(\chi^{(2)}_{xxz}) = \mathrm{Im}(\chi^{(2)}_{yyz})$, $\mathrm{Im}(\chi^{(2)}_{yzy})$, and $\mathrm{Im}(\chi^{(2)}_{zzz})$ spectra (denoted as A_{yyz}, A_{yzy}, and A_{zzz}, respectively) are related via

$$A_{yyz}:A_{yzy}:A_{zzz} = [(1+R)D-(1-R)]:(1-R)(D-1):2(RD+1-R), \quad (4)$$

where R represents the depolarization ratio for the target vibrational mode and D is the parameter related with the molecular orientation [19].

A closer inspection of Eqs. (1)–(4) suggests that the peak amplitude in the $\chi^{(2)}_{zzz}$ spectrum, A_{zzz}, can be obtained using two fully independent approaches: (i) Using Eqs. (1) and (3), one can obtain the $\chi^{(2)}_{zzz}$ spectrum from the measured $\chi^{(2)}_{\mathrm{eff},ssp}$ and $\chi^{(2)}_{\mathrm{eff},ppp}$ spectra, providing A_{zzz}. (ii) Using Eqs. (1) and (2), one can obtain $\chi^{(2)}_{yyz}$ and $\chi^{(2)}_{yzy}$ spectra from the measured $\chi^{(2)}_{\mathrm{eff},ssp}$ and $\chi^{(2)}_{\mathrm{eff},sps}$ spectra, providing A_{yyz} and A_{yzy}, respectively. By using Eq. (4), A_{zzz} can be obtained from A_{yyz} and A_{yzy}. The precise values of A_{zzz} obtained from approaches (i) and (ii) depend on the value of the interfacial dielectric constant ε' in Eqs. (1)–(3). In other words, through the comparison of A_{zzz}, one can access the interfacial dielectric constant.

Because the interfacial dielectric constant is depth dependent [20], SFG can provide information on the average position of the vibrational chromophores, if ε' can be linked with depth. We derive the relation of ε' and the position of the chromophore, z at the air-liquid interface within the embedded model of a vibrational chromophore [inset of Fig. 1(b)] [18,21]. The interfacial dielectric constant ε' at position z is given as [21]

$$\varepsilon' = \begin{cases} \varepsilon & \text{for } z \le -r, \\ \frac{1+\frac{1}{3}(1-\frac{\varphi}{\pi})(\varepsilon-1)}{1+(\frac{1-\varepsilon}{6\varepsilon})(1+\frac{z}{r})^2(2-\frac{z}{r})} & \text{for } -r < z \le r, \\ 1 & \text{for } z > r, \end{cases} \quad (5)$$

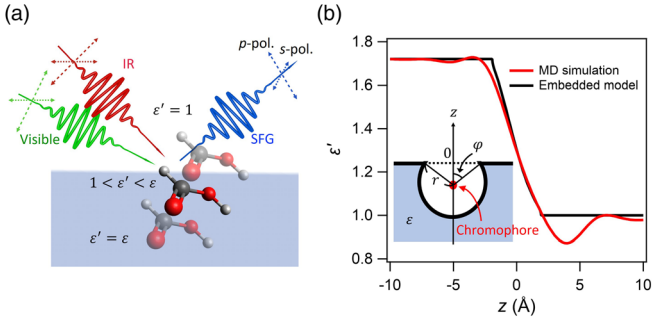

FIG. 1. (a) Schematic for PD-SFG spectroscopy probing a formic acid molecule at the air-water interface. ε and ε' are the bulk and interface dielectric constant of formic acid solution, respectively. (b) Depth profile of ε' at the air-water interface in the optical limit ($\varepsilon = 1.72$). The black line is obtained from Eq. (5), while the red line represents the MD simulation result obtained from Ref. [20]. Note that the impact of the surface roughness was removed from the depth profile of ε' through the deconvolution. The inset schematic represents the vibrational chromophore (red dot) at the interface. φ is the angle between the surface normal and the vector pointing from the center of the sphere to the crossing point of the dielectric interface and the surface of the sphere. r is the radius of the vibrational chromophore. The origin point of the z axis is the position where the chromophore experiences $\varepsilon' = \varepsilon(\varepsilon+5)/(4\varepsilon+2)$ [21].

where φ is the angle between the surface normal and the vector pointing from the center of the sphere to the crossing point of the dielectric interface and the surface of the sphere. r is the radius of the vibrational chromophore. $z = 0$ denotes the location where the chromophore experiences $\varepsilon' = \varepsilon(\varepsilon+5)/(4\varepsilon+2)$ ($\varphi = \pi/2$) [21]. Note that $\varphi = 0$ and $\pi/2$ provide the interfacial dielectric constants within the Lorentz and slab models, respectively [21–23].

Let us check whether Eq. (5) can reproduce the variation of the dielectric profile as a function of depth which the molecular dynamics (MD) simulation predicts at the air-water interface [20]. Here, we set $\varepsilon = 1.72$ in the optical limit and employed $r = 1.93$ Å, where the value of r was determined by the average volume of the water molecules in the bulk. The resulting depth profile of ε' displayed in Fig. 1(b), together with results from the MD simulation [20]. These data largely agree, indicating that Eq. (5) provides a reliable description of the depth-dependent dielectric function experienced by a vibrational chromophore at the air-water interface.

We examined whether our proposed PD-HD-SFG methodology can probe the depth position of the C—H stretch chromophores of the formic acid molecule at the air-formic acid solution interface. We measured the SFG spectra in the C—H stretch mode of the SFG active formic acid molecules at the air-formic acid solution interfaces at ssp, sps, and ppp polarization combinations. Experimental $\mathrm{Im}\chi^{(2)}_{\mathrm{eff},ssp}$, $\mathrm{Im}\chi^{(2)}_{\mathrm{eff},sps}$, and $\mathrm{Im}\chi^{(2)}_{\mathrm{eff},ppp}$ spectra with various x_{FA} are displayed in Figs. 2(a)–2(c), respectively. First, we

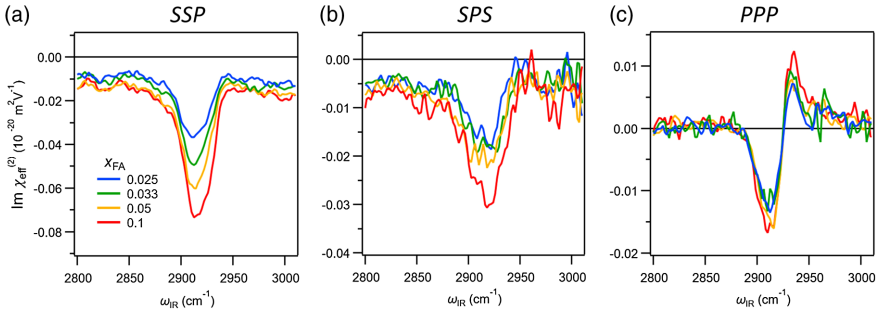

FIG. 2. Experimental (a) $\mathrm{Im}\chi^{(2)}_{\mathrm{eff},ssp}$, (b) $\mathrm{Im}\chi^{(2)}_{\mathrm{eff},sps}$, and (c) $\mathrm{Im}\chi^{(2)}_{\mathrm{eff},ppp}$ spectra at the air-formic acid solution interface in the C—H stretch mode region with various x_{FA}.

focus on the $\mathrm{Im}\chi^{(2)}_{\mathrm{eff},ssp}$ spectra. The spectra commonly show the 2920 cm^{-1} negative peak and ~2880 cm^{-1} negative shoulder feature. The 2920 and 2880 cm^{-1} features can be assigned to the C—H stretch mode of formic acid molecules' trans and cis conformations, respectively [24–26]. Since the spectral contribution of the 2880 cm^{-1} feature is much smaller than the 2920 cm^{-1} contribution, we did not analyze the 2880 and 2920 cm^{-1} contributions separately. The negative signs of the $\mathrm{Im}\chi^{(2)}_{\mathrm{eff},ssp}$ peaks indicate that the C → H group points *up* toward the vapor phase [27]. This can be rationalized by the inability of the hydrophobic C—H group to form a hydrogen bond with water.

Subsequently, we discuss the $\mathrm{Im}\chi^{(2)}_{\mathrm{eff},sps}$ and $\mathrm{Im}\chi^{(2)}_{\mathrm{eff},ppp}$ spectra. The $\mathrm{Im}\chi^{(2)}_{\mathrm{eff},sps}$ spectra resemble the $\mathrm{Im}\chi^{(2)}_{\mathrm{eff},ssp}$ spectra, while the $\mathrm{Im}\chi^{(2)}_{\mathrm{eff},ppp}$ spectra show positive features at ~2930 cm^{-1}, unlike the $\mathrm{Im}\chi^{(2)}_{\mathrm{eff},sps}$ and $\mathrm{Im}\chi^{(2)}_{\mathrm{eff},ssp}$ spectra, due to the slight frequency shift between the $\chi^{(2)}_{zzz}$ and $\chi^{(2)}_{yyz}$ spectra; the frequency shift gives rise to the negative-positive feature in the $\mathrm{Im}\chi^{(2)}_{\mathrm{eff},ppp}$ spectra, because the $\mathrm{Im}\chi^{(2)}_{\mathrm{eff},ppp}$ spectra arise from the subtraction of the $\chi^{(2)}_{zzz}$ from the $\chi^{(2)}_{yyz}$ contribution (see Supplemental Material [28]).

From the $\mathrm{Im}\chi^{(2)}_{\mathrm{eff},ssp}$, $\mathrm{Im}\chi^{(2)}_{\mathrm{eff},sps}$, and $\mathrm{Im}\chi^{(2)}_{\mathrm{eff},ppp}$ spectra, one can obtain the $\mathrm{Im}\chi^{(2)}_{yyz}$, $\mathrm{Im}\chi^{(2)}_{yzy}$, and $\mathrm{Im}\chi^{(2)}_{zzz}$ spectra at different averaged depth z. Here, we used the dielectric constant of the formic acid-H_2O mixtures, with interfacial formic acid concentrations inferred from the SFG spectra of heavy water's hydrogen bonded O—D band (see Supplemental Material [28]). The peak amplitudes A_{yyz}, A_{yzy}, and A_{zzz} for the C—H stretch mode were obtained by integrating the peak areas in the $\mathrm{Im}\chi^{(2)}_{yyz}$, $\mathrm{Im}\chi^{(2)}_{yzy}$, and $\mathrm{Im}\chi^{(2)}_{zzz}$ spectra, respectively. Finally, we obtained A_{zzz} via approach (i) and approach (ii), where we used $R = 0.13$ [26]. The data using approach (i) are displayed as solid lines in Fig. 3(a), while the data using approach (ii) are depicted as dotted lines as a function of the depth z [see also Fig. 1(b)]. The crossing points of the solid and dotted lines marked with an "×" in Fig. 3(a) represent the averaged depth position of the C—H stretch vibrational chromophores. The robustness of our approach is discussed in detail in Supplemental Material [28].

Our analysis indicates that the SFG active C—H stretch chromophores were located at the topmost layer at low concentration $x_{\mathrm{FA}} = 0.025$ ($z = -0.5$ Å). Since the C—H group of formic acid molecules are hydrophobic, locating the formic acid molecules at the topmost layer minimizes the system's free energy [45,46]. When increasing x_{FA} from 0.025 to 0.1, the average position of the C—H chromophores shifts toward the bulk by ~0.9 Å [see Fig. 3(b)].

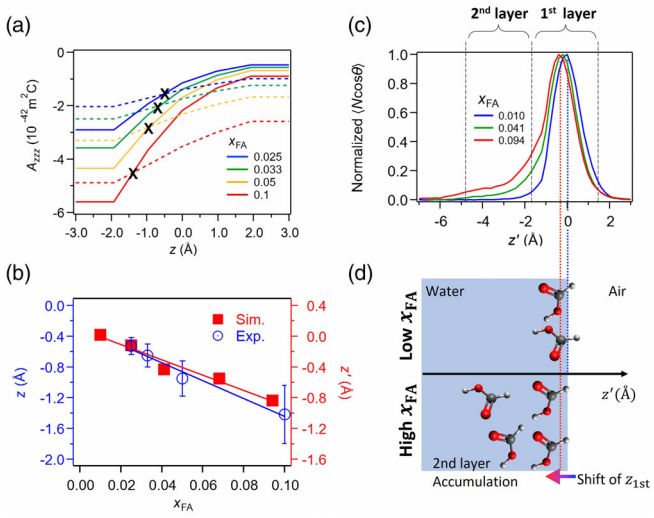

FIG. 3. (a) The amplitude A_{zzz} as a function of the averaged depth position of the chromophore. The solid lines and dotted lines are obtained using approaches (i) and (ii), respectively. The "×" marks denote the crossing points of the solid and dotted lines, indicating the depth position of the C—H stretch vibrational chromophore. (b) Comparison of the position shift of the C—H stretch chromophore between experiment and simulation. The lines serve to guide the eye. The error bars correspond to the uncertainty based on the dielectric constant for the bulk and surface concentrations (see Supplemental Material [28]). (c) Normalized simulated depth profile of the $\langle N \cos\theta \rangle$ at different x_{FA}. (d) Schematics of formic acid absorption at the air-formic acid solution interface at different x_{FA}. Note that only SFG-active formic acid molecules are depicted here.

To confirm the observation that the position of the C—H vibrational chromophore is shifted by ~0.9 Å upon increasing x_{FA} from 0.025 to 0.10, we compared this position shift with the MD simulation data at the air-formic acid solution interfaces [46]. The depth positions z' of the C—H stretch vibrational chromophores of the formic acid were computed based on the instantaneous liquid interface description, where $z' = 0$ provides the position of the instantaneous liquid interface [47] (see Supplemental Material [28]). To highlight the SFG active formic acid molecules, we computed the depth profiles of $\langle N \cos\theta \rangle$ instead of the profiles of formic acid density [46] (see Supplemental Material [28]). Where N is the number of the C—H bonds and θ represents the angle formed by the C → H bond and the surface normal pointing to air, the depth profiles of $\langle N \cos\theta \rangle$ at different x_{FA} are displayed in Fig. 3(c). These profiles show that, with increasing x_{FA}, the relative population in the second layer increases as well as a slight shift in the peak position in the first layer, lowering the averaged position of the SFG active stretch chromophore (see Supplemental Material [28]).

To quantitatively compare the position of the C—H chromophore between experiment and simulation, we summarize the shift of its averaged position in Fig. 3(b). Experiments and simulation agree very well, manifesting that the PD-HD-SFG spectroscopy scheme can accurately capture the change in the average position of the vibrational chromophores. Furthermore, this agreement leads to the molecular picture that the position of the outermost formic acid monolayer shifts toward the bulk with increasing x_{FA}, while the other mechanism is that accumulation of the formic acid molecules in the second and third layers leads to the shift of the average position [Fig. 3(d)].

In conclusion, we have developed a novel methodology to obtain the Ångstrom-scale depth information using SFG measurements at ssp, sps, and ppp polarization combinations. By using this methodology, SFG becomes an interface-specific, molecular-specific, and depth-sensitive technique. We demonstrated that the method allows us to access to the depth information of the C—H stretch chromophores of formic acid molecules at the air-formic acid solution interface. Increasing the formic acid fraction leads to a shift of the position of the chromophore from the topmost interface to the bulk region. Furthermore, quantitative agreement between MD simulations and the polarization-dependent SFG experiments suggests that this shift results from a combination of a shifting formic acid monolayer at the topmost water layer into the bulk and multilayer adsorption with increasing bulk concentration. The proposed technique can be used to probe the depth information on various molecules and materials, including biomolecules and 2D materials [48–51].

We acknowledge the financial support from the MaxWater Initiative of the Max Planck Society. We thank Shumei Sun, Masanari Okuno, and Johannes Hunger for fruitful discussion.

The authors declare no competing interests.

*These authors contributed to this work equally.
†Corresponding author.
bonn@mpip-mainz.mpg.de
‡Corresponding author.
nagata@mpip-mainz.mpg.de

[1] O. Björneholm, M. H. Hansen, A. Hodgson, L. M. Liu, D. T. Limmer, A. Michaelides, P. Pedevilla, J. Rossmeisl, H. Shen, G. Tocci, E. Tyrode, M. M. Walz, J. Werner, and H. Bluhm, Chem. Rev. **116**, 7698 (2016).
[2] K. T. Nguyen and A. V. Nguyen, Langmuir **35**, 4825 (2019).
[3] T. Seki, S. Sun, K. Zhong, C. C. Yu, K. Machel, L. B. Dreier, E. H. G. Backus, M. Bonn, and Y. Nagata, J. Phys. Chem. Lett. **10**, 6936 (2019).
[4] A. Senes, D. C. Chadi, P. B. Law, R. F. S. Walters, V. Nanda, and W. F. DeGrado, J. Mol. Biol. **366**, 436 (2007).
[5] A. L. Lomize, I. D. Pogozheva, M. A. Lomize, and H. I. Mosberg, Protein Sci. **15**, 1318 (2006).
[6] A. G. Lee, Trends Biochem. Sci. **36**, 493 (2011).
[7] H.-J. Butt, K. Graf, and M. Kappl, *Physics and Chemistry of Interfaces* (Wiley, New York, 2003).
[8] J. S. Fletcher, N. P. Lockyer, and J. C. Vickerman, Mass Spectrom. Rev. **30**, 142 (2011).
[9] S. Ghosal, J. C. Hemminger, H. Bluhm, B. S. Mun, E. L. D. Hebenstreit, G. Ketteler, D. F. Ogletree, F. G. Requejo, and M. Salmeron, Science **307**, 563 (2005).
[10] K. Vedam, P. J. McMarr, and J. Narayan, Appl. Phys. Lett. **47**, 339 (1985).
[11] Q. Du, R. Superfine, E. Freysz, and Y. R. Shen, Phys. Rev. Lett. **70**, 2313 (1993).
[12] M. Bonn, Y. Nagata, and E. H. G. Backus, Angew. Chem., Int. Ed. Engl. **54**, 5560 (2015).
[13] L. Fu, G. Ma, and E. C. Y. Yan, J. Am. Chem. Soc. **132**, 5405 (2010).
[14] T. Seki, X. Yu, P. Zhang, C.-C. Yu, K. Liu, L. Gunkel, R. Dong, Y. Nagata, X. Feng, and M. Bonn, Chem **7**, 2758 (2021).
[15] D. S. Walker, D. K. Hore, and G. L. Richmond, J. Phys. Chem. B **110**, 20451 (2006).
[16] E. A. Raymond, T. L. Tarbuck, M. G. Brown, and G. L. Richmond, J. Phys. Chem. B **107**, 546 (2003).
[17] T. L. Tarbuck and G. L. Richmond, J. Am. Chem. Soc. **128**, 3256 (2006).
[18] A. Morita, *Theory of Sum Frequency Generation Spectroscopy* (Springer, Singapore, 2018).
[19] X. Wei and Y. R. Shen, Phys. Rev. Lett. **86**, 4799 (2001).
[20] K. Shiratori and A. Morita, J. Chem. Phys. **134**, 234705 (2011).
[21] X. Zhuang, P. B. Miranda, D. Kim, and Y. R. Shen, Phys. Rev. B **59**, 12632 (1999).

[22] J. D. Jackson, *Classical Electrodynamics*, 3rd ed. (Wiley, New York, 1998).
[23] X. Wei, S. C. Hong, X. Zhuang, T. Goto, and Y. R. Shen, Phys. Rev. E **62**, 5160 (2000).
[24] K. Marushkevich, L. Khriachtchev, and M. Räsänen, J. Phys. Chem. A **111**, 2040 (2007).
[25] E. M. S. Maçôas, J. Lundell, M. Pettersson, L. Khriachtchev, R. Fausto, and M. Räsänen, J. Mol. Spectrosc. **219**, 70 (2003).
[26] C.-C. Yu, S. Imoto, T. Seki, K.-Y. Chiang, S. Sun, M. Bonn, and Y. Nagata, J. Chem. Phys. **156**, 094703 (2022).
[27] S. Nihonyanagi, S. Yamaguchi, and T. Tahara, J. Chem. Phys. **130**, 204704 (2009).
[28] See Supplemental Material at http://link.aps.org/supplemental/10.1103/PhysRevLett.128.226001 for experimental and simulation procedures, derivation of the interfacial dielectric constant, the dielectric constant for the bulk and surface molar fraction of formic acid solution, and additional SFG data, including the estimation of the surface fraction of formic acid solution and the discussion of the second layer accumulation of formic acid inferred from O─D stretch SFG data, which includes Refs. [29–44].
[29] J. Sung, K. Park, and D. Kim, J. Phys. Chem. B **109**, 18507 (2005).
[30] W. Sung, S. Seok, D. Kim, C. S. Tian, and Y. R. Shen, Langmuir **26**, 18266 (2010).
[31] J. Wang, Z. Paszti, M. A. Even, and Z. Chen, J. Am. Chem. Soc. **124**, 7016 (2002).
[32] J. Ho, B. T. Psciuk, H. M. Chase, B. Rudshteyn, M. A. Upshur, L. Fu, R. J. Thomson, H. F. Wang, F. M. Geiger, and V. S. Batista, J. Phys. Chem. C **120**, 12578 (2016).
[33] H. Vanselous and P. B. Petersen, J. Phys. Chem. C **120**, 8175 (2016).
[34] M. J. Abraham, T. Murtola, R. Schulz, S. Páll, J. C. Smith, B. Hess, and E. Lindahl, SoftwareX **2**, 19 (2015).
[35] W. L. Jorgensen, D. S. Maxwell, and J. Tirado-Rives, J. Am. Chem. Soc. **118**, 11225 (1996).
[36] J. L. F. Abascal, E. Sanz, R. García Fernández, and C. Vega, J. Chem. Phys. **122**, 234511 (2005).
[37] I. V. Stiopkin, C. Weeraman, P. A. Pieniazek, F. Y. Shalhout, J. L. Skinner, and A. V. Benderskii, Nature (London) **474**, 192 (2011).
[38] C.-S. Tian and Y. R. Shen, J. Am. Chem. Soc. **131**, 2790 (2009).
[39] M. Sovago, R. K. Campen, G. W. H. Wurpel, M. Müller, H. J. Bakker, and M. Bonn, Phys. Rev. Lett. **100**, 173901 (2008).
[40] E. A. Raymond and G. L. Richmond, J. Phys. Chem. B **108**, 5051 (2004).
[41] Y. Nagata, R. E. Pool, E. H. G. Backus, and M. Bonn, Phys. Rev. Lett. **109**, 226101 (2012).
[42] P. A. Pieniazek, C. J. Tainter, and J. L. Skinner, J. Chem. Phys. **135**, 044701 (2011).
[43] T. Ishiyama and A. Morita, J. Phys. Chem. C **111**, 721 (2007).
[44] J. E. Bertie, M. K. Ahmed, and H. H. Eysel, J. Phys. Chem. **93**, 2210 (1989).
[45] C. M. Johnson, E. Tyrode, A. Kumpulainen, and C. Leygraf, J. Phys. Chem. C **113**, 13209 (2009).
[46] X. Yu, T. Seki, C.-C. Yu, K. Zhong, S. Sun, M. Okuno, E. H. G. Backus, J. Hunger, M. Bonn, and Y. Nagata, J. Phys. Chem. B **125**, 10639 (2021).
[47] A. P. Willard and D. Chandler, J. Phys. Chem. B **114**, 1954 (2010).
[48] J. Kaur, M. Singh, C. Dell'Aversana, R. Benedetti, P. Giardina, M. Rossi, M. Valadan, A. Vergara, A. Cutarelli, A. M. I. Montone, L. Altucci, F. Corrado, A. Nebbioso, and C. Altucci, Sci. Rep. **8**, 16386 (2018).
[49] M. Singh, C. Zannella, V. Folliero, R. DiGirolamo, F. Bajardi, A. Chianese, L. Altucci, A. Damasco, M. R. DelSorbo, C. Imperatore, M. Rossi, M. Valadan, M. Varra, A. Vergara, G. Franci, M. Galdiero, and C. Altucci, Front. Bioeng. Biotechnol. **8**, 569967 (2020).
[50] J. Wang, X. Chen, M. L. Clarke, and Z. Chen, Proc. Natl. Acad. Sci. U.S.A. **102**, 4978 (2005).
[51] M. Xiao, S. Wei, Y. Li, J. Jasensky, J. Chen, C. L. Brooks, and Z. Chen, Chem. Sci. **9**, 1769 (2018).